

# Chemical Science

Accepted Manuscript

This article can be cited before page numbers have been issued, to do this please use: X. Pei, W. Wu, Y. Sun, Q. Yang, J. Weng, S. Zhang, Z. Geng and B. Zhu, *Chem. Sci.*, 2026, DOI: 10.1039/D6SC00984K.



This is an Accepted Manuscript, which has been through the Royal Society of Chemistry peer review process and has been accepted for publication.

Accepted Manuscripts are published online shortly after acceptance, before technical editing, formatting and proof reading. Using this free service, authors can make their results available to the community, in citable form, before we publish the edited article. We will replace this Accepted Manuscript with the edited and formatted Advance Article as soon as it is available.

You can find more information about Accepted Manuscripts in the [Information for Authors](#).

Please note that technical editing may introduce minor changes to the text and/or graphics, which may alter content. The journal's standard [Terms & Conditions](#) and the [Ethical guidelines](#) still apply. In no event shall the Royal Society of Chemistry be held responsible for any errors or omissions in this Accepted Manuscript or any consequences arising from the use of any information it contains.

# Direct Arylation Polymerization of Electron-Rich Arenes with Polar-Group Tolerance Enabled by Ligand-Coordination Tuning

Xilin Pei<sup>1,2,3,4</sup>, §, Wei Wu<sup>1,3,4</sup>, §, Yanlu Sun<sup>5</sup>, Quan Yang<sup>1,3,4</sup>, Jianan Weng<sup>1,3,4</sup>, Shuhua Zhang<sup>1,3,4</sup>, Zhi Geng<sup>1,3,4</sup>, Bo Zhu<sup>1,3,4</sup> \*

1. School of Materials Science and Engineering, Shanghai University, Shanghai 200444, China.
2. State Key Laboratory for Modification of Chemical Fibers and Polymer Materials, Innovation Center for Textile Science & Technology, College of Material Science and Engineering, Donghua University, Shanghai 201620, China.
3. Shanghai Engineering Research Center of Organ Repair, Shanghai University, Shanghai 200444, China.
4. Joint International Research Laboratory of Biomaterials and Biotechnology in Organ Repair, Ministry of Education
5. College of Textiles, Donghua University, Shanghai 201620, China.

§ These authors contributed equally: Xilin Pei, Wei Wu.



## Abstract

View Article Online  
DOI: 10.1039/D6SC00984K

Electron-rich arenes are crucial building blocks in conjugated polymers due to their strong electron-donating properties and tunable electronic structures, underpinning diverse applications in organic electronics, biointerfaces, and energy technologies. However, the pronounced  $\pi$ -delocalization of electron-rich arenes can increase the arene distortion and reorganization energy required at the transition state, making efficient C-H activation under typical phosphine conditions challenging, particularly when polar substituents simultaneously compete for Pd coordination. The absence of a comprehensive mechanistic understanding of interactions among ligands, catalysts, arenes, and polar substituents has forced researchers to rely on empirical condition screening, significantly limiting synthetic efficiency and the scope of functional polymers. Using 3,4-ethylenedioxythiophene (EDOT) and its derivatives as representative electron-rich monomers, we demonstrate that the phosphine ligand coordination strength, quantified by electron-donating strength (EDS), critically governs both the C-H activation efficiency and the catalyst's tolerance toward polar groups. Weak-donating ligands facilitate Pd-C formation and disrupt localized  $\pi$ -delocalization, significantly enhancing C-H activation. Conversely, the more donating ligands within the weak-donating series, strengthen Pd-phosphine interaction relative to Pd-polar-group coordination, shifting the coordination balance away from inhibitory polar-group-bound Pd states and thereby mitigating catalyst poisoning. This mechanistic insight provides a predictive framework for rational condition selection in DArP, replacing empirical screening with a design-driven strategy. The resulting protecting-group-free strategy provides scalable access to high-molecular-weight conjugated polymers bearing diverse functionalities, including the notoriously catalyst-deactivating amines, and expands the synthetic toolkit for functional conjugated polymers in organic electronics, biointerfaces, and energy applications.

## Keywords

Electron-rich arenes; direct arylation polymerization; functional group tolerance; conjugated polymers



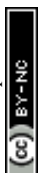
## Introduction

View Article Online  
DOI: 10.1039/D6SC00984K

3,4-Ethylenedioxythiophene (EDOT) is a central electron-rich building block for conducting and semiconducting polymers. EDOT-based polymers, especially PEDOT and its derivatives, are widely used in organic electronics, bioelectronics, sensing, and energy-related devices because of their redox stability, electrical conductivity, electrochemical robustness, and mixed ionic-electronic transport<sup>1-14</sup>. Introducing polar substituents such as hydroxyl, carboxyl, or amine groups into EDOT-based polymers is attractive because these groups can improve processability, tune interfacial interactions, modulate charge transfer, and provide chemical handles for further functionalization. However, the protecting-group-free synthesis of high-molecular-weight polar-functionalized EDOT polymers remains difficult because it requires efficient C-H activation of the electron-rich EDOT core while simultaneously managing polar substituents that can affect solubility, alter catalyst coordination, and deactivate transition-metal catalysts<sup>15, 16</sup>.

Direct arylation polymerization (DARp) is particularly appealing for EDOT-based polymer synthesis because it forms aryl-aryl bonds directly from arene C-H bonds and aryl halides, avoiding the organometallic monomers required in Stille, Suzuki, and Kumada polymerizations<sup>17-24</sup>. Several DARp protocols have enabled the polymerization of EDOT-type monomers, demonstrating that EDOT arylation is feasible under optimized catalytic conditions<sup>25-29</sup>. Nevertheless, these successes remain largely condition-specific, and a predictive framework for selecting ligands for polar-functionalized EDOT monomers remains lacking. This limitation becomes critical when hydroxyl, carboxyl, or amine groups are introduced, because catalyst performance then depends not only on C-H activation efficiency but also on resistance to nonproductive coordination by polar substituents.

In Pd-catalyzed direct arylation, C-H cleavage commonly proceeds through a concerted metalation-deprotonation (CMD) pathway, in which the Pd center and a coordinated carboxylate, such as pivalate, cooperate to cleave the C-H bond<sup>30-32</sup>. Importantly, CMD is not governed by arene electron density in the manner expected for electrophilic aromatic substitution; both electron-rich and electron-poor arenes can undergo CMD-based activation when the catalyst environment is properly matched to the substrate. Therefore, EDOT-type monomers should not be viewed as intrinsically unreactive. Rather, our calculations suggest that EDOT's pronounced  $\pi$ -delocalization



can increase the arene distortion and  $\pi$ -bond reorganization required to reach the CMD transition state.

Moreover, polar substituents introduce an additional, mechanistically distinct complication. Heteroatom-containing groups can serve as directing groups in small-molecule C-H activation, but under DArP conditions, they may instead act as competitive ligands that bind Pd in off-cycle states and suppress catalytic turnover<sup>33-39</sup>. Primary amines are particularly problematic because their strong  $\sigma$ -donating ability and high affinity for Pd(II) can severely deactivate the catalyst. Protecting groups can mask these interactions, but they add synthetic steps and reduce the step-economy advantage of DArP.

Here, we address this challenge through ligand-coordination-tuned DArP using polar-functionalized EDOT derivatives as representative monomers. Across eleven phosphine ligands, combined experimental and computational analyses identify phosphine electron-donating strength (EDS) as a practical descriptor that regulates both CMD-based C-H activation and tolerance toward coordinating polar groups. More weakly donating ligands strengthen Pd(4d)-C(2p) interaction at the CMD intermediate and transition state, promoting Pd-C bond formation and the arene distortion that locally disrupts  $\pi$ -delocalization. More donating ligands, in contrast, strengthen Pd-phosphine coordination relative to Pd-polar-group coordination, shifting the coordination equilibrium away from persistent off-cycle polar-group-bound Pd species. Balancing these opposing effects through precise tuning of ligand EDS explains why ligands with moderate-donating strength achieve optimal performance, simultaneously enabling efficient arene activation and DArP and minimizing catalyst deactivation. This mechanistic framework shifts ligand selection in DArP of electron-rich arenes from empirical trial-and-error toward rational and design-driven synthesis. We envision that the resulting ligand-coordination-tuned approach provides a general, sustainable, and predictive strategy for accessing diverse high-molecular-weight conjugated EDOT polymers, significantly expanding synthetic capabilities and advancing materials development in organic electronics, biointerfaces, and energy applications.

## Results and Discussion

### Modulating DArP of EDOT monomers via ligand electron-donating strength

We selected eleven monophosphine ligands, including strong-donating alkyl



phosphines (L1-L3), moderate-donating aryl phosphines (L4-L6), and weak-donating aryl phosphines (L7-L11), as ligands for the Pd catalyst to activate the C-H bonds of electron-rich EDOT derivatives and polymerize them. We first evaluated their EDS qualitatively by measuring the coupling constants ( $J_{\text{Rh-P}}$ ) in the  $^{31}\text{P}$  NMR spectra of their complexes with rhodium ( $[\text{RhCl}(\text{CO})(\text{Ln})_2]$ ) (Figure 2B), as a weaker coordination strength typically leads to a higher  $J_{\text{Rh-P}}$ <sup>40</sup>. However, for L6, its methoxy substituent competes with the phosphorus atom to interact with rhodium, reducing the phosphorus's contribution and causing  $J_{\text{Rh-P}}$  to deviate. In addition to electronic properties, the steric profile of the ligands (particularly those with aryl ortho-substituents, i.e., L5, L6, L7, and L11) also influences their coordination behavior.

The functionalized EDOT-based polymers were synthesized via a general palladium-catalyzed cross-coupling polymerization. The degree of polymerization (DP) of the hydroxyl-functionalized EDOT (EDOT-OH) and EDOT copolymers (PEE-OH), synthesized at 120 °C for 1 hr (L4-L11), was determined using solution-state  $^1\text{H}$  NMR spectroscopy, as GPC measurements did not yield reliable results, likely due to column adsorption caused by hydrazine, which was used to reduce the polymers and improve their solubility. DPs increased dramatically with the  $J_{\text{Rh-P}}$  values of the ligands L4-L11 (Figures 2C and D). Specifically, weak-donating ligands were associated with significantly higher polymer yields and degrees of polymerization than the more strongly donating ligands. Their UV-Vis spectra confirmed this trend, demonstrating a general red shift in  $\lambda_{\text{max}}$  with higher  $J_{\text{Rh-P}}$  values (Figure 2E), consistent with the extended conjugation typical of higher molecular weights in conjugated polymers. The yields for those reactions with weak-donating ligands were also higher. No products were available with the strong-donating alkyl-phosphine ligands (L1-L3).

The DP value of the polymer synthesized with the L11 ligand was 30, with an 88 % yield. To verify this unique ligand effect with a different aryl bromide, we replaced 2,5-dibromo-3,4-ethylenedioxythiophene with 1,4-dibromobenzene and synthesized its copolymer with EDOT-OH (PPE-OH) by reacting them at 120 °C for 1 hr. The weak-donating ligands again produced polymers with much higher molecular weights and higher yields (Figure 2F). The DP value of PPE-OH, which differed from that of PEE-OH, exhibited exponential growth as the  $J_{\text{Rh-P}}$  value increased (Figure 2G). The UV results further verified this trend (Figure 2H). This result indicated that the PPE-OH growth was more sensitive to the ligand EDS than the PEE-OH growth. We attribute



this enhanced sensitivity to the electron deficiency and weak coordinating ability of benzene relative to EDOT, which mimics the behavior of weak-donating ligands. The DP reached an impressive value of 972, with a 92% yield, when using L11. Additionally, no significant side-group interference was detected during the polymerization of PEE-OH and PPE-OH. Furthermore, PPE-OH was polymerized via DArP under ligandless conditions (a DP of 108) and with azacyclo-auxiliary ligands (e.g., pyridine, resulting in a DP of 9), both of which demonstrated substantially lower polymerization efficiency compared to using L11. This result suggests that tuning the ligand EDS, particularly when using phosphine-based ligands, plays a critical role in enhancing polymerization performance.

To further evaluate the L11 conditions, we examined PEE-OH at extended reaction time and PPE-OH at shortened reaction time. The DP of PEE-OH increased significantly to 86, with a 91% yield after extending the reaction time to 24 hrs (Table S3). PPE-OH still achieved a high DP value of 176, with an 83% yield after reducing the reaction time to 30 mins (Table S4). These results demonstrate, respectively, the durability and reactivity of the L11-based system. Additionally, the DPs of PEE-OH (86) after 24 hrs and PPE-OH (972) after 1 hr under L11 conditions are significantly higher than those obtained under ligand-free conditions (77 and 108, respectively), despite identical reaction parameters (Tables S3/S4).

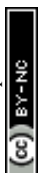
To benchmark our L11 system against efficient DArP conditions reported for EDOT-type monomers, we performed comparative experiments using literature-adapted Pd<sub>2</sub>(dba)<sub>3</sub>/o-methoxytriphenylphosphine (L6)/PivOH/toluene conditions<sup>26, 41-43</sup>. For PEE-OH, the benchmark system using 2 mol% Pd<sub>2</sub>(dba)<sub>3</sub>, 4 mol% L6, Cs<sub>2</sub>CO<sub>3</sub>, and PivOH in toluene at 110 °C gave DPs of 23 and 29 after 1 and 48 h, with yields of 31% and 32%, respectively (Table S3), lower than the DP of 86 obtained with L11. For PPE-OH, the same benchmark conditions gave DPs of 14 and 17 after 1 and 48 h, respectively (Table S4), far below the DP of 972 achieved with L11.

A higher-loading variant of the L6/toluene system using 10 mol% Pd<sub>2</sub>(dba)<sub>3</sub>, 20 mol% L6, and KPivO led to extensive toluene-derived end-capping or solvent incorporation for both PEE-OH and PPE-OH, making reliable DP determination difficult. In contrast, the L11/Pd(OAc)<sub>2</sub>/DMAc/KPivO system showed no detectable solvent- or ligand-derived incorporation and afforded higher-DP polymers with cleaner end-group behavior.



We then used carboxyl-functionalized EDOT (EDOT-COOH) as an arylation substrate instead to synthesize copolymers with EDOT/benzene (PEE-COOH/PPE-COOH) and found that L5, L6, L7, and L11 gave no products (Figures 3A and B). A common feature of these ligands was their ortho substituents on their phenyl rings, which provided significant steric hindrance to prevent EDOT-COOH from approaching. As evaluated by the Tolman cone angles<sup>44, 45</sup>, the ortho-substituted phosphine ligands with cone angles  $\geq 135^\circ$ , i.e., L5, L6, L7, and L11, gave no PEE-COOH or PPE-COOH product, while L10, with a slightly smaller cone angle of  $134^\circ$ , retained partial activity (Figure 3C). We considered that under basic conditions, EDOT-COOH would complex with Pd through the carboxylate and ester oxygen to form a stable five-membered chelate (Figure 3D) and thus amplify the steric effect of the ligands on the reactivities of intermediates<sup>36</sup>. PEE-COOH and PPE-COOH only dissolved in aqueous hydrazine. However, it is difficult to measure their molecular weights from the  $^1\text{H}$  NMR spectra of their aqueous solutions, as the diagnostic  $\alpha$ -proton resonance of the terminal EDOT unit cannot be observed, plausibly because of H/D exchange with the deuterated solvent. The similar UV absorption maxima of PEE-COOHs suggest comparable conjugation lengths under the tested conditions, likely limited by poor solubility in DMAc. In contrast, the red-shifted absorption of PPE-COOHs with decreasing ligand EDS qualitatively indicates extended conjugation and more efficient EDOT-COOH arylation under selected ligand conditions, consistent with the weak-ligand-enhanced activation trend discussed above (Figures 3E and 3F).

Activating the primary amine-functionalized arene remains a considerable challenge, as it competes with the arene substrates for tight coordination with Pd, typically deactivating the Pd catalyst. Consistent with this expectation, the copolymer of amine-functionalized EDOT (EDOT-NH<sub>2</sub>) with EDOT (PEE-NH<sub>2</sub>) gave low DPs and yields under the conditions optimized for PEE-OH (L7 and L11), even when the reaction time was extended to 6 h (Figures 3G and I). The small molecule model also confirmed that the L7 and L11 conditions are inactive in arylating EDOT-NH<sub>2</sub> with 2-bromo-5-methylthiophene and bromobenzene (Figures S2 and S3). As ligand EDS increased, however, the DPs of PEE-NH<sub>2</sub> rose sharply, implying partial or complete release of primary amine groups from the Pd catalyst. After the DPs and yields reached their maximum at L9, they decreased with further increases in ligand EDS. A similar phenomenon was also observed in synthesizing the copolymer of EDOT-NH<sub>2</sub> and



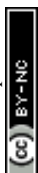
benzene (PPE-NH<sub>2</sub>) (Figure 3H). A striking DP (711) was achieved for PPE-NH<sub>2</sub> synthesized with L8, with a yield of 73%. Furthermore, this unique dependence of molecular weight on EDS was further confirmed by the results of the 1 hr and 3 hr reactions (Tables S7 and S8).

To determine whether this volcano-shaped trend reflects intrinsic arylation chemistry rather than polymerization-specific effects, we conducted model reactions of EDOT-NH<sub>2</sub> with 2-bromo-5-methylthiophene or bromobenzene under analogous conditions. These reactions reproduced the same ligand dependence, with L7 and L11 showing little activity, L8 and L9 giving the highest EDOT-NH<sub>2</sub> consumption, and more donating ligands such as L4 showing reduced activity (Figure S5). Because these model reactions do not involve chain growth, the trend cannot be mainly attributed to chain-extension kinetics, solubility changes, or accumulation of amine-containing repeat units.

We propose that amine coordination is also strongly influenced by the ligand's EDS but in a manner opposite to the DArP activity of electron-rich arenes, necessitating a trade-off between the two processes to facilitate efficient polymerization. Accordingly, the highest DPs for both the EDOT-NH<sub>2</sub> copolymers were achieved using an optimized ligand with a medium EDS (Figures 3I and J). These results highlight the importance of balancing between the amine coordination and the DArP activity of electron-rich arenes by tuning the ligand's EDS to overcome amine-induced catalyst poisoning. Matched-cone-angle comparisons (Tables S7 and S8) further show that the ligand effect cannot be explained by steric effects alone, as L8 greatly outperforms L4 in PPE-NH<sub>2</sub>, despite nearly identical cone angles, and L9 similarly outperforms L4 in PEE-NH<sub>2</sub>. This electronic-effect explanation is further supported by the ligand-free benchmark, which gave moderate activity for PEE-OH and PPE-OH polymerization but only low DPs (3 and 20) and yields (23% and 41%) for PEE-NH<sub>2</sub> and PPE-NH<sub>2</sub>, respectively (Tables S7 and S8).

### Weak ligand coordination promotes deprotonation

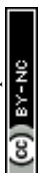
To uncover the unique effect of ligand EDS on the DArP activity of electron-rich EDOT substrates, we employed DFT to compute Gibbs free-energy profiles for the C-H activation step across the L4–L11 ligand series, focusing on the concerted metalation-deprotonation (CMD) pathway as the operative mechanism. A typical CMD process for the C-H activation of EDOT alpha carbon, where two intermediates (Pre-TS and Post-



TS) occur before and after the transition state (TS)<sup>46</sup>, is shown in Figure 4A. The  $\Delta G^\ddagger$  values for both direct arylations of EDOT with EDOT and benzene reached the minimum when the weakest-donating ligand (L11) was used (Tables S10 and S12). These results strongly corroborate the experimental findings, underscoring the pivotal role of the ligand EDS in facilitating the C-H activation of electron-rich EDOT derivatives.

To gain deeper insight into the CMD processes, we performed natural bond orbital (NBO) analysis on the EDOT-EDOT coupling at both the Pre-TS and TS stages. The more weakly donating ligands (those with higher  $J_{\text{Rh-P}}$  values) corresponded to lower Wiberg bond orders (WBOs) for the Pd-P bond at Pre-TS. This weakening of the Pd-P interaction coincided with a strengthened Pd-C bond, directly supporting the notion that weaker ligands promote stronger Pd-C bonding (Figure 4B). A similar trend was observed at the TS stage, where both Pd-C and Pd-P WBOs showed a consistent dependence on ligand EDS. Consistent results were also obtained from the NBO analysis of EDOT-benzene coupling, further reinforcing the observed trends (Figure 4C). We also conducted NAO analyses to decompose the Pd-P and Pd-C WBOs<sup>47, 48</sup>, and found that the Pd-P WBO primarily arises from hybridization between the Pd 4d and P 3p orbitals, while the Pd-C WBO is mainly due to hybridization between the Pd 4d and C 2p orbitals. Analysis of their dependences on ligand electron-donating strength (EDS) revealed that decreasing the ligand EDS weakens Pd(4d)-P(3p) hybridization while strengthening Pd(4d)-C(2p) hybridization (Figure 4D). A comparable trend was observed in the NAO analysis of the coupling between EDOT and benzene substrates (Figure 4E). All the above findings indicate that reducing ligand EDS promotes Pd-C bond formation by attenuating the Pd-P interaction.

The EDOT distortion energies at the Pre-TS for both the EDOT-EDOT and EDOT-benzene couplings are directly proportional to the corresponding Pd-C $\alpha$  WBOs (Figures 4F and G), consistent with the observation that both the distortion energies (Figure S6) and Pd-C $\alpha$  WBOs (Figures 4B and C) at the Pre-TS exhibit linear correlations with the ligand EDS. This key finding supports the conclusion that stronger Pd-C bonds, resulting from weakened Pd-P interactions, lead to more pronounced EDOT distortion. We further found that this characteristic EDOT distortion at the Pre-TS with the weak-donating ligand (L11) directly coincides with a significant reduction in localized  $\pi$ -delocalization near C $\alpha$ , as evidenced by comparisons between EDOT and



Pre-TS EDOT in the second and fourth highest occupied molecular orbitals (HOMO-2 and HOMO-3) (Figure 4H; Tables S27 and S28). To better understand this phenomenon, we analyzed the correlation between the contribution of  $C\alpha(2p_z)$ - $C\beta(2p_z)$  orbital hybridization to  $\pi$ -delocalization in the pre-transition state (Pre-TS) and the Pd- $C\alpha$  WBOs, revealing a clear inverse linear relationship (Figures 4I and J).

Based on these results, we propose that decreasing ligand EDS attenuates Pd(4d)-P(3p) hybridization and allows greater Pd(4d)-C(2p) interaction between the Pd(II) intermediate and the electron-rich EDOT  $C\alpha$  carbon, thereby strengthening Pd-C bond formation during CMD. This interaction distorts the C-H bond and diminishes the adjacent  $\pi$ -delocalization, in turn facilitating proton shuttling from EDOT substrates to the carboxylates. The same EDS principle also rationalizes the inactivity of the strong-donating alkyl phosphines L1-L3 in the EDOT-rich PEE series, where insufficient activation of the EDOT C-H bond becomes the dominant limitation. This mechanistic insight provides predictive guidance for rational ligand design to achieve high molecular weight EDOT polymers, offering greater flexibility in addressing compatibility challenges associated with polar side groups, as discussed below.

### Mitigating catalyst poisoning of polar groups

Heteroatoms bearing lone electron pairs can compete with the arene substrate for coordination at Pd, lowering reactivity and deactivating the catalyst. No catalyst poisoning was observed for the EDOT-OH polymerization, consistent with the weakly coordinating nature of the hydroxyl group (Figure 5A). In contrast, polymerization of EDOT-COOH was completely suppressed when ortho-substituted aryl-phosphine ligands were used (Figures 3A and B). This result was attributed to the enhanced steric sensitivity of the Pd(II) catalyst once the five-membered carboxylate chelate has formed by the complexation of EDOT-COOH with Pd under basic conditions (Figure 5B). However, weak-donating ligands of reduced steric profile (e.g., L9) can alleviate the geometric constraint imposed by the five-membered chelate, allowing productive Pd- $C\alpha$  bond formation. In this regime, the Pd-bound EDOT-COOH does not need to dissociate; instead, its carboxylate functions as the proton-shuttle ligand for CMD.

Not surprisingly, EDOT-NH<sub>2</sub> exhibited the strongest catalyst poisoning due to its robust coordination with Pd, forming a stable mono-amine Pd(II) complex (Figure 5C). This complexation substantially suppressed catalytic activity, resulting in poor yields



and low molecular weights for the copolymers of EDOT-NH<sub>2</sub> with EDOT or benzene substrates when synthesized under conditions (L7 and L11) optimized for the EDOT-OH copolymer (Figures 3G and H). This issue was mitigated by L8 and L9, the more donating members of the weak-donating ligand class, which strengthen Pd-phosphine interaction relative to the most weakly donating ligands L7 and L11, while retaining sufficient weak-donating character to support CMD-based EDOT activation (Figures 3I and J).

We hypothesized that ligands with relatively stronger donating character within the productive series, i.e., higher EDS than L7 and L11, would promote dissociation of the Pd-amine bond by enhancing the competing Pd-phosphine interaction. To verify this, we performed NBO analyses on mono-amine Pd(II) complexes. The NBO analysis of the mono-amine Pd(II) complexes shows that, as ligand EDS increases, the Pd-phosphine Wiberg bond order rises while the Pd-amine WBO falls in parallel, with the two trends strongly negatively correlated for both EDOT-EDOT and EDOT-benzene couplings (Figures 5D-G). This coordination-sphere redistribution shifts the catalyst away from persistent Pd-amine-bound off-cycle states.

Therefore, ligand EDS not only tunes the electronic environment of the Pd center but also governs the suppression of catalyst poisoning by polar functional groups such as amines. By promoting selective dissociation of inhibitory ligands through competitive coordination, the moderately donating ligands within the weak-donating class (L8 and L9) restore the catalytic competence of Pd(II) and enable efficient polymerization. This mechanistic insight is particularly significant for expanding the substrate scope of direct arylation polymerization (DARp) to include functionalized arenes, thus providing a foundation for rational design of conjugated polymers with diverse polar side chains and tailored properties.

## Conclusions

In this study, we systematically elucidated, through experimental and computational investigations, how phosphine ligands interact with electron-rich EDOT derivatives and diverse polar side groups through coordination to Pd. We further showed how the electronic nature of these ligands dictates both arene activation and catalyst deactivation in DARp. By parameterizing ligand coordination strength in terms of EDS, we show that more weakly donating phosphines enhance Pd-C bond formation and attenuate local  $\pi$ -delocalization, thereby promoting C-H activation. However, weaker ligand



donation also makes the Pd catalyst more susceptible to coordination by polar groups, which can lead to catalyst deactivation. Further analyses show that catalyst poisoning from strongly coordinating side groups, such as amines, can be effectively mitigated by employing the moderately donating ligands within the weak-donating class. These ligands redistribute the Pd coordination sphere toward stronger Pd-phosphine interaction relative to Pd-amine coordination, helping mitigate amine-induced catalyst poisoning and restore catalytic turnover. Striking this optimal balance through precise tuning of ligand EDS proved essential for overcoming the dual challenges of activating electron-rich arenes and suppressing deactivation caused by polar functionalities. Finally, this ligand-coordination-tuned strategy enables the synthesis of high-molecular-weight functionalized conjugated polymers with excellent tolerance to hydroxyl and amine groups, as well as moderate, ligand-dependent compatibility with carboxylic acid functionalities that is sensitive to both steric and electronic ligand effects. This mechanistic clarification of how ligand electronic properties govern both DArP reactivity and catalyst stability establishes a predictive framework for rational ligand selection, transforming ligand design from empirical trial-and-error into a design-driven strategy. These findings advance the mechanistic understanding of DArP for electron-rich arenes and provide a versatile platform for synthesizing functional conjugated polymers with tailored side groups for organic electronics, biointerfaces, and energy applications.

## Experimental

### Polymer synthesis via DArP

The monomers, including 2,5-dibromo-3,4-ethylenedioxythiophene (DBEDOT), hydroxyl-functionalized EDOT (EDOT-OH), carboxyl-functionalized EDOT (EDOT-COOH), and amine-functionalized EDOT (EDOT-NH<sub>2</sub>), were synthesized according to previously reported procedures<sup>49-51</sup>. For polymer synthesis, a general method was employed: in a glovebox, a Schlenk tube was charged with functionalized EDOT monomer (1 equiv), arene dibromide (1 equiv), palladium acetate (10 mol%), potassium pivalate (2 equiv), phosphine ligand (20 mol%), and DMAc (0.125 M monomer) at a 0.25 mmol scale, along with a magnetic stir bar. The mixture was heated in an oil bath at the specified temperature with vigorous stirring for a specified time, then cooled to ambient temperature. Full polymerization details are available in the Supporting



Information.

View Article Online  
DOI: 10.1039/D6SC00984K

## Calculation methods

All quantum chemical calculations were performed using Gaussian 09<sup>52</sup>. Density functional theory (DFT) at the M06L level<sup>53</sup> was employed: geometry optimizations and frequency analyses were performed using the SDD basis set for Pd and 6-31G(d) for all other atoms. Single-point energy calculations were then conducted with SDD for Pd and 6-311++G(d,p) for the remaining atoms. Gibbs free energy corrections were obtained by combining these single-point energies with thermal corrections from the frequency calculations, and solvation effects were included using the PCM model with DMAc as solvent to describe the concerted metalation-deprotonation process. Transition states were verified by intrinsic reaction coordinate (IRC) calculations. Electrostatic potential (ESP) mapping, Tolman cone angle estimation<sup>54</sup>, frontier orbital visualization, and Wiberg bond order evaluation based on natural bond orbital (NBO) and natural atomic orbital (NAO) were further carried out<sup>55</sup>. Full computational details are provided in the Supporting Information.

## ASSOCIATED CONTENT

### Supporting Information

General methods, experimental procedures, NMR spectra, and calculational details.

### Author Contributions

B.Z. and X.P. initiated the project and designed the experiments. X.P., W.W., Q.Y. synthesized the monomers and polymers and characterized these materials. X.P., S.Y., J.W. characterized these materials. X.P., B.Z., conducted the computations and mechanistic analysis. X.P., B.Z. wrote the initial draft. B.Z., X.P., S.Z., and Z.G. revised the manuscript. B.Z. supervised the work.

### Notes

The authors declare no competing interests.

### Acknowledgements



We gratefully acknowledge the High Performance Computing Center of Shanghai University and the Shanghai Engineering Research Center of Intelligent Computing System for providing computational resources and support. B.Z. acknowledges the financial support from the NSFC (22175111, 21474014). Z.G. acknowledges the financial support from the NSFC (21704013).

## References:

1. T. Someya, Z. Bao and G. G. Malliaras, *Nature*, 2016, 540, 379–385.
2. Z. Zhang, W. Wang, Y. Jiang, Y. X. Wang, Y. Wu, J. C. Lai, S. Niu, C. Xu, C. C. Shih, C. Wang, H. Yan, L. Galuska, N. Prine, H. C. Wu, D. Zhong, G. Chen, N. Matsuhisa, Y. Zheng, Z. Yu, Y. Wang, R. Dauskardt, X. Gu, J. B. Tok and Z. Bao, *Nature*, 2022, 603, 624–630.
3. A. J. Gillett, A. Privitera, R. Dilmurat, A. Karki, D. Qian, A. Pershin, G. Londi, W. K. Myers, J. Lee, J. Yuan, S.-J. Ko, M. K. Riede, F. Gao, G. C. Bazan, A. Rao, T.-Q. Nguyen, D. Beljonne and R. H. Friend, *Nature*, 2021, 597, 666–671.
4. Y. Wang, C. Zhu, R. Pfattner, H. Yan, L. Jin, S. Chen, F. Molina-Lopez, F. Lissel, J. Liu, N. I. Rabiah, Z. Chen, J. W. Chung, C. Linder, M. F. Toney, B. Murmann and Z. Bao, *Sci. Adv.*, 2017, 3, e1602076.
5. Y. Jiang, Z. Zhang, Y.-X. Wang, D. Li, C.-T. Coen, E. Hwanun, G. Chen, H.-C. Wu, D. Zhong and S. Niu, *Science*, 2022, 375, 1411–1417.
6. B. Zhu, S. C. Luo, H. Zhao, H. A. Lin, J. Sekine, A. Nakao, C. Chen, Y. Yamashita and H. H. Yu, *Nat. Commun.*, 2014, 5, 4523.
7. T. J. Quill, G. LeCroy, D. M. Halat, R. Sheelamanthula, A. Marks, L. S. Grundy, I. McCulloch, J. A. Reimer, N. P. Balsara, A. Giovannitti, A. Salleo and C. J. Takacs, *Nat. Mater.*, 2023, 22, 362–368.
8. A. Elschner, k. Stephan, W. Lovenich, U. Merker and K. Kreuter, *PEDOT: Principles and Applications of an Intrinsically Conductive Polymer*, Wiley, 2010.
9. H. Dong, E. Zheng, Z. Niu, X. Zhang, Y.-Y. Lin, P. Jain and Q. Yu, *ACS Appl. Mater. & Interfaces*, 2020, 12, 17571–17582.
10. H. Yano, K. Kudo, K. Marumo and H. Okuzaki, *Sci. Adv.*, 2019, 5, eaav9492.
11. X. Strakosas, H. Biesmans, T. Abrahamsson, K. Hellman, M. S. Ejneby and o. D. Mary J. , *Science*, 2023, 379, 795–802.
12. N. Li, Y. Li, Z. Cheng, Y. Liu, Y. Dai, S. Kang, S. Li, N. Shan, S. Wai and A. Ziaji, *Science*, 2023, 381, 686–693.
13. M. Hjort, A. H. Mousa, D. Bliman, M. A. Shameem, K. Hellman, A. S. Yadav, P. Ekström, F. Ek and R. Olsson, *Nat. Commun.*, 2023, 14, 4453.
14. P. D. Howes, R. Chandrawati and M. M. Stevens, *Science*, 2014, 346, 1247390.
15. A. H. Mousa, D. Bliman, L. Hiram Betancourt, K. Hellman, P. Ekstrom, M. Savvakis, X. Strakosas, G. Marko-Varga, M. Berggren, M. Hjort, F. Ek and R. Olsson, *Chem. Mater.*, 2022, 34, 2752–2763.
16. K. Wang, G. Wang and M. Wang, *Macromol. Rapid Commun.*, 2015, 36, 2162–2170.
17. S. Cheng, R. Zhao and D. S. Seferos, *Acc. Chem. Res.*, 2021, 54, 4203–4214.
18. B. Carsten, F. He, H. J. Son, T. Xu and L. Yu, *Chem. Rev.*, 2011, 111, 1493–1528.



19. H. Xiong, Q. Lin, Y. Lu, D. Zheng, Y. Li, S. Wang, W. Xie, C. Li, X. Zhang, Y. Lin, Z.-X. Wang, Q. Shi, T. J. Marks and H. Huang, *Nat. Mater.*, 2024, 23, 695–702. View Article Online  
DOI: 10.1039/D3SC00984K
20. N. S. Gobalasingham and B. C. Thompson, *Prog. Polym. Sci.*, 2018, 83, 135–201.
21. A. L. Mayhugh, P. Yadav and C. K. Luscombe, *J. Am. Chem. Soc.*, 2022, 144, 6123–6135.
22. J.-R. Pouliot, F. Grenier, J. T. Blaskovits, S. Beaupré and M. Leclerc, *Chem. Rev.*, 2016, 116, 14225–14274.
23. X. Zhang, Y. Shi, Y. Deng and Y. Geng, *Chin. J. Chem.*, 2023, 41, 2908–2924.
24. S. J. Gilman, S. Saiev, J.-L. Brédas and J. R. Reynolds, *Macromolecules*, 2025, 58, 4807–4818.
25. F. Grenier, K. Goudreau and M. Leclerc, *J. Am. Chem. Soc.*, 2017, 139, 2816–2824.
26. Z.-R. Tan, Y.-Q. Xing, J.-Z. Cheng, G. Zhang, Z.-Q. Shen, Y.-J. Zhang, G. Liao, L. Chen and S.-Y. Liu, *Chem. Sci.*, 2022, 13, 1725–1733.
27. F. Grenier, B. R. Aïch, Y.-Y. Lai, M. Guérette, A. B. Holmes, Y. Tao, W. W. H. Wong and M. Leclerc, *Chem. Mater.*, 2015, 27, 2137–2143.
28. C. Wang, C. J. Mueller, E. Gann, A. C. Y. Liu, M. Thelakkat and C. R. McNeill, *J. Mater. Chem. A*, 2016, 4, 3477–3486.
29. X.-L. Pei, Q. Yang, Y.-L. Sun, W. Wu, J.-Y. Yu and Y. He, *Chinese Journal of Polymer Science*, 2025, 43, 718–729.
30. M. Lafrance, C. N. Rowley, T. K. Woo and K. Fagnou, *J. Am. Chem. Soc.*, 2006, 128, 8754–8756.
31. D. Lapointe and K. Fagnou, *Chem. Lett.*, 2010, 39, 1118–1126.
32. S. I. Gorelsky, D. Lapointe and K. Fagnou, *J. Org. Chem.*, 2011, 77, 658–668.
33. B. Xiao, T. J. Gong, Z. J. Liu, J. H. Liu, D. F. Luo, J. Xu and L. Liu, *J. Am. Chem. Soc.*, 2011, 133, 9250–9253.
34. D. Posevins, Y. Qiu and J. E. Backvall, *J. Am. Chem. Soc.*, 2018, 140, 3210–3214.
35. P. X. Shen, L. Hu, Q. Shao, K. Hong and J. Q. Yu, *J. Am. Chem. Soc.*, 2018, 140, 6545–6549.
36. Z. Wang, L. Hu, N. Chekshin, Z. Zhuang, S. Qian, J. Qiao and J.-Q. Yu, *Science*, 2021, 374, 1281–1285.
37. Z. Zhuang and J.-Q. Yu, *J. Am. Chem. Soc.*, 2020, 142, 12015–12019.
38. S. Z. Ali, B. G. Budaitis, D. F. A. Fontaine, A. L. Pace, J. A. Garwin and M. C. White, *Science*, 2022, 376, 276–283.
39. J. Calleja, D. Pla, T. W. Gorman, V. Domingo, B. Haffemayer and M. J. Gaunt, *Nat. Chem.*, 2015, 7, 1009–1016.
40. T. Korenaga, A. Ko, K. Uotani, Y. Tanaka and T. Sakai, *Angew. Chem. Int. Ed.*, 2011, 50, 10703–10707.
41. Z.-H. Xie, G. Ye, H. Gong, P. Murugan, C. Lang, Y.-F. Dai, K. Yang and S.-Y. Liu, *Chem. Sci.*, 2025, 16, 9998–10009.
42. B. Zhang, Y. Cai, L. He, N. Xu, Y. Yuan, J. Zhang, Y. Zhang and P. Wang, *Chem. Sci.*, 2024, 15, 17103–17113.
43. H. Gong, J. Li, Z.-H. Xie, C. Lang and S.-Y. Liu, *Macromolecules*, 2024, 57, 7208–7218.
44. C. A. Tolman, *Chem. Rev.*, 1977, 77, 313–348.
45. S. Zhao, T. Gensch, B. Murray, Z. L. Niemeyer, M. S. Sigma and M. R. Biscoe, *Science*, 2018, 362, 670–674.
46. S. I. Gorelsky, D. Lapointe and K. Fagnou, *J. Org. Chem.*, 2012, 77, 658–668.
47. T. Lu and F. Chen, *Acta Chim. Sinica*, 2011, 69, 2393–2406.
48. T. Lu and F. Chen, *J. Comput. Chem.*, 2012, 33, 580–592.



49. Y. Q. Zhang, H. A. Lin, Q. C. Pan, S. H. Qian, S. H. Zhang, G. Qiu, S. C. Luo, H. H. Yu and B. Zhu, *ACS Appl, Mater, Interfaces*, 2020, 12, 12362–12372. [View Article Online](#)  
DOI: 10.1039/D6SC00984K
50. W. Zhang, R. Jamal, R. Zhang, Z. Yu, Y. Yan, Y. Liu, Y. Ge and T. Abdiryim, *Phys. Chem. Chem. Phys.*, 2020, 22, 3592–3603.
51. Meng Hong, Perepichka Dmitrii F. and Wudl Fred, *Angew. Chem. Int. Ed.*, 2003, 42, 589–589.
52. M. J. Frisch, G. W. Trucks, H. B. Schlegel, G. E. Scuseria, M. A. Robb, J. R. Cheeseman, G. Scalmani, V. Barone, B. Mennucci, G. A. Petersson, H. S211 Nakatsuji, M. Caricato, X. Li, H. P. Hratchian, A. F. Izmaylov, J. Bloino, G. Zheng, J. L. Sonnenberg, M. Hada, M. Ehara, K. Toyota, R. Fukuda, J. Hasegawa, M. Ishida, T. Nakajima, Y. Honda, O. Kitao, H. Nakai, T. Vreven, J. A. Montgomery, Jr., J. E. Peralta, F. Ogliaro, M. Bearpark, J. J. Heyd, E. Brothers, K. N. Kudin, V. N. Staroverov, T. Keith, R. Kobayashi, J. Normand, K. Raghavachari, A. Rendell, J. C. Burant, S. S. Iyengar, J. Tomasi, M. Cossi, N. Rega, J. M. Millam, M. Klene, J. E. Knox, J. B. Cross, V. Bakken, C. Adamo, J. Jaramillo, R. Gomperts, R. E. Stratmann, O. Yazyev, A. J. Austin, R. Cammi, C. Pomelli, J. W. Ochterski, R. L. Martin, K. Morokuma, V. G. Zakrzewski, G. A. Voth, P. Salvador, J. J. Dannenberg, S. Dapprich, A. D. Daniels, O. Farkas, J. B. Foresman, J. V. Ortiz, J. Cioslowski, and D. J. Fox, *Gaussian 09, Revision E.01*, Gaussian, Inc., Wallingford CT, 2013.
53. Y. Zhao and D. G. Truhlar, *J. Chem. Phys.*, 2006, 125, 194101.
54. I. A. Guzei and M. Wendt, *Dalton T.*, 2006, 33, 3991–3999.
55. E. D. Glendening, A. E. Reed, J. E. Carpenter, and F. Weinhold, *NBO Version 3.1*.



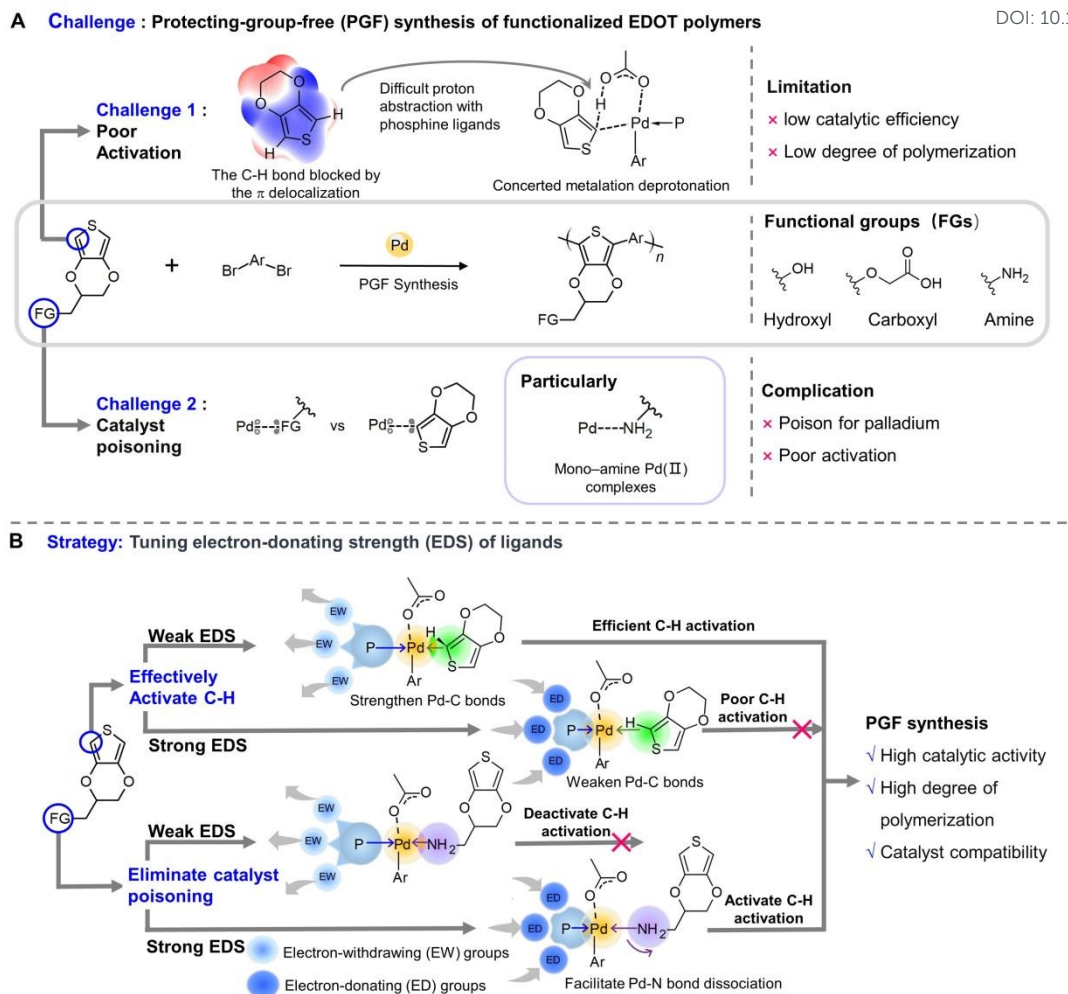


**Figure 1. ligand-coordination-tuned direct arylation polymerization for synthesizing functionalized EDOT polymers. (A) The two challenges for the synthesis of functionalized EDOT polymers by palladium-catalyzed direct arylation polymerization are poor activation of electron-rich EDOT derivatives and catalyst poisoning of side polar groups. (B) Tuning the electron-donating strength of phosphine ligands facilitates the concerted metalation-deprotonation of EDOTs and direct arylation polymerization of functionalized EDOT polymers.**



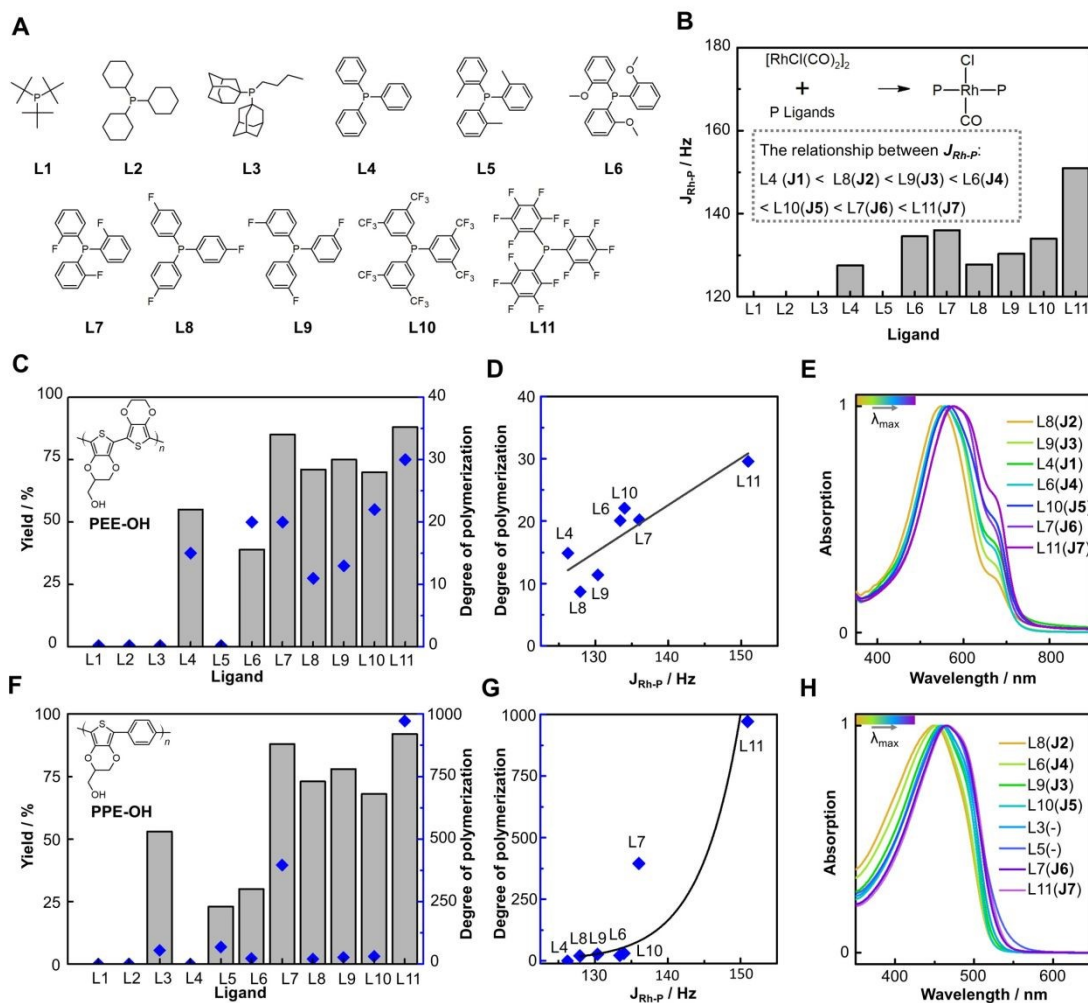


**Figure 2.** Effect of ligands' electron-donating strength (EDS) on the direct arylation polymerization of hydroxyl functionalized EDOT (EDOT-OH). **(A)** The phosphine ligands used in this study. **(B)** EDS values of aryl-phosphine ligands evaluated by the coupling constants ( $J_{Rh-P}$ ) of  $[RhCl(CO)(L_n)_2]_2$  in their  $^{31}P$  NMR spectra. **(C)** The degrees of polymerization (DPs) and the yields of the copolymers of EDOT-OH with EDOT (PEE-OHs) synthesized using the phosphine ligands shown in Figure 2A. PEE-OHs were synthesized on a 0.25 mmol scale using EDOT-OH (1 eq.), dibromo-EDOT (1 eq.),  $Pd(OAc)_2$  (10 mol %), phosphine ligand (20 mol %), and  $KPivO$  (2 eq.) in DMAc (0.125 M) at 120 °C for 1 hr. **(D)** The plot of the PEE-OH DPs as a function of  $J_{Rh-P}$ . **(E)** The UV spectra of PEE-OHs in DMSO/N<sub>2</sub>H<sub>4</sub>·H<sub>2</sub>O (85 %) (v/v = 100:1). **(F)** The DPs and the yields for the copolymers of EDOT-OH with benzene (PPE-OHs) synthesized using the phosphine ligands shown in Figure 2A. PPE-OHs were synthesized on a 0.25 mmol scale using EDOT-OH (1 eq.), dibromobenzene (1 eq.),  $Pd(OAc)_2$  (10 mol %), phosphine ligand (20 mol %), and  $KPivO$  (2 eq.) in DMAc (0.125 M) at 120 °C for 1 hr. **(G)** The plot of the PPE-OH DPs as a function of  $J_{Rh-P}$ . **(H)** The UV spectra of PPE-OHs in DMSO/N<sub>2</sub>H<sub>4</sub>·H<sub>2</sub>O.



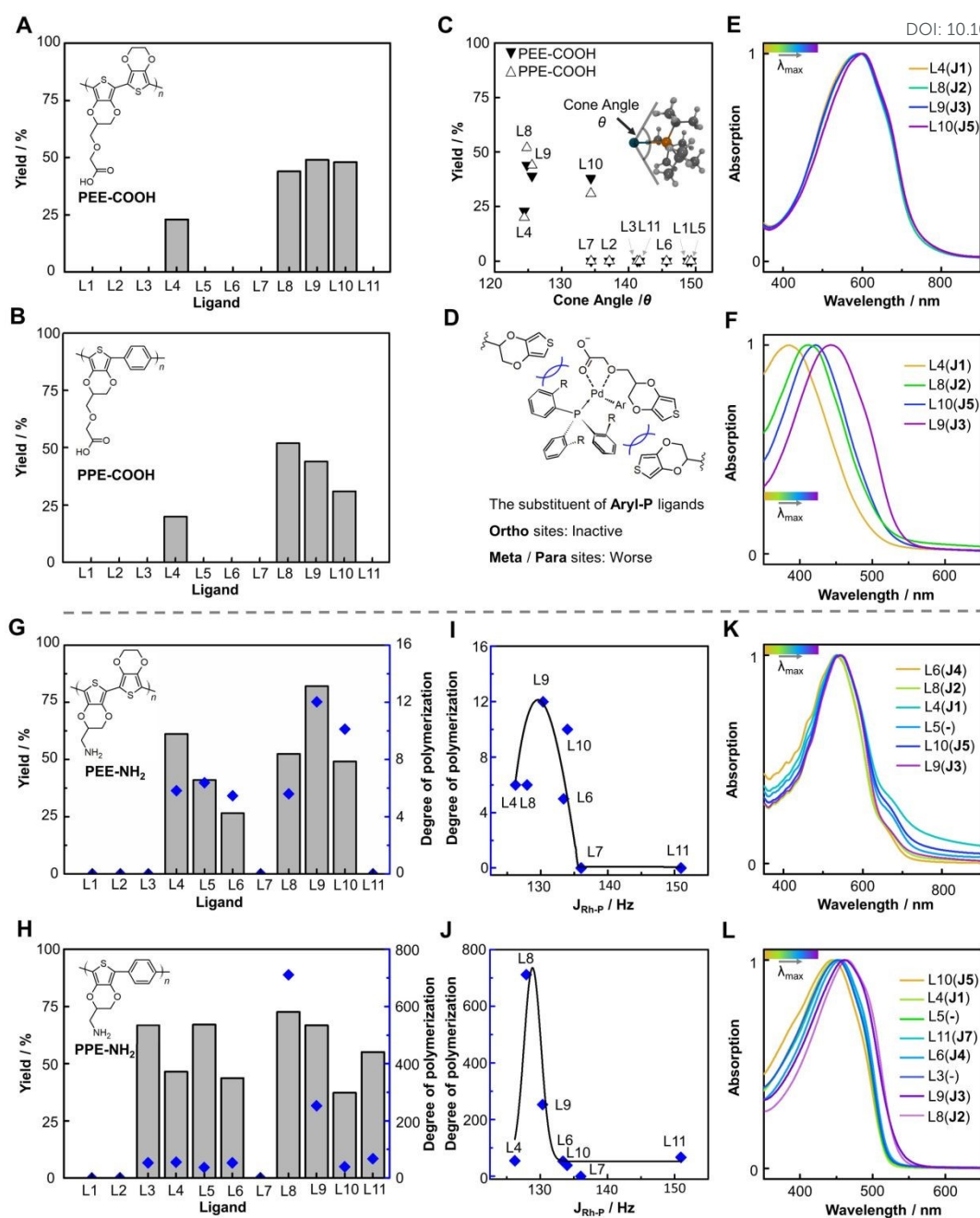


**Figure 3. Compatibility of carboxyl and amine groups with palladium catalyst in direct arylation polymerization. (A and B)** The yield for (A) the copolymers of EDOT-COOH with EDOT (PEE-COOHs) and (B) those of EDOT-COOH with benzene (PPE-COOHs) using phosphine ligands listed in Figure 2A. PEE-COOHs and PPE-COOHs were synthesized on a 0.25 mmol scale using EDOT-COOH (1 eq.), arene dibromide (1 eq.), Pd(OAc)<sub>2</sub> (10 mol %), phosphine ligand (20 mol %) and KPIvO (2 eq.) in DMAc (0.125 M) at 120 °C for 1 hr. (C) The plot of the yields of PEE-COOHs and PPE-COOHs as a function of the cone angle of phosphine ligands. The embedded graph illustrates the Tolman cone-angle representation for L1, with the M-P distance fixed at 2.28 Å. The geometry optimization of phosphine ligands was done using M06L/6-31G(d), and the Tolman cone angles were calculated by Solid-G software. (D) Schematic illustration of how ortho-substituents on the aryl-phosphine ligands sterically block approach of the EDOT-COOH substrate to the Pd center. (E and F) The UV spectra of the synthesized (E) PEE-COOHs and (F)



PPE-COOHs in  $N_2H_4 \cdot H_2O$  (85 %) solutions. **(G and H)** The DPs and the yields for **(G)** the copolymer of EDOT-NH<sub>2</sub> with EDOT (PEE-NH<sub>2</sub>) and **(H)** that of EDOT-NH<sub>2</sub> with benzene (PPE-NH<sub>2</sub>) using phosphine ligands listed in Figure 2A. PEE-NH<sub>2</sub> and PPE-NH<sub>2</sub>s were synthesized on a 0.25 mmol scale using EDOT-NH<sub>2</sub> (1 eq.), arene dibromide (1 eq.), Pd(OAc)<sub>2</sub> (10 mol %), phosphine ligand (20 mol %) and KPivO (2 eq.) in DMAc (0.125 M) at 120 °C for 6 hrs. **(I and J)** The plots of the **(I)** PEE-NH<sub>2</sub> DPs and the **(J)** PPE-NH<sub>2</sub> DPs as a function of  $J_{Rh-P}$ . **(K and L)** The UV spectra of the synthesized **(K)** PEE-NH<sub>2</sub> and **(L)** PPE-NH<sub>2</sub> in DMSO /  $N_2H_4 \cdot H_2O$  (85 %) (v/v = 100:1).

View Article Online  
DOI: 10.1039/D6SC00984K



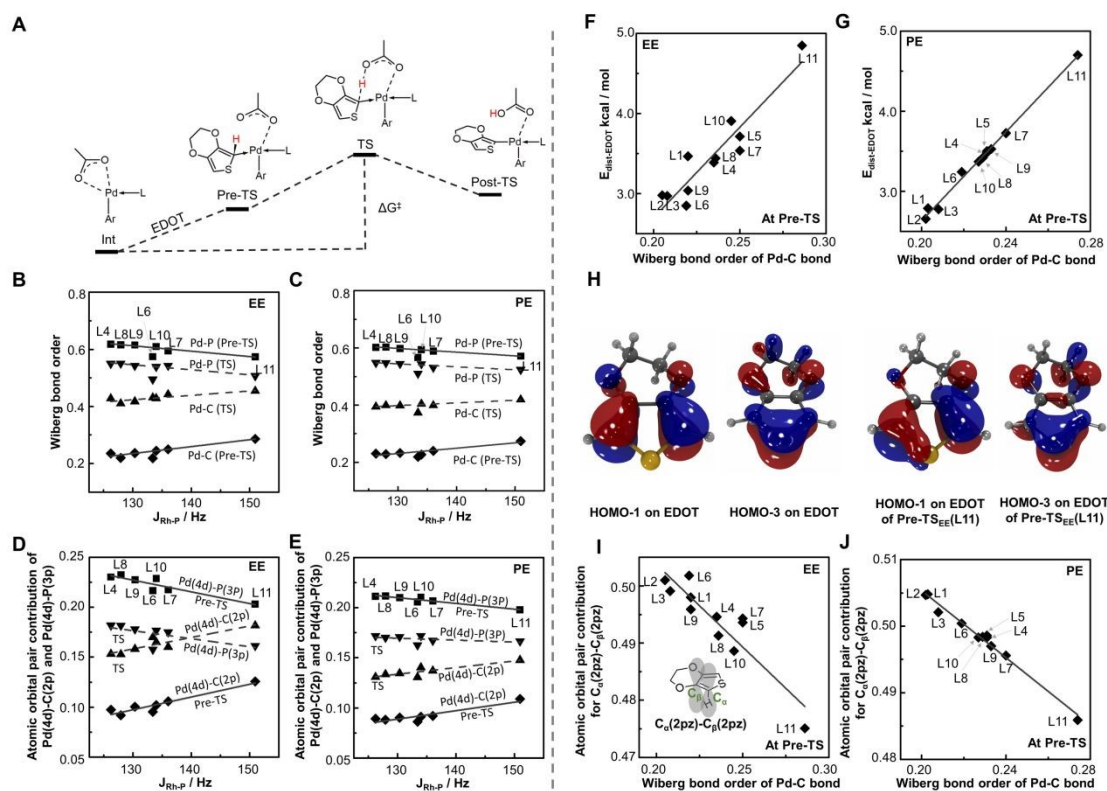


**Figure 4. Weak ligand coordination facilitates deprotonation.** (A) The typical concerted metalation-deprotonation (CMD) pathway for EDOT activation, where a prior intermediate (Pre-TS) occurs ahead of the transition state (TS). (B and C) The plots of the Wiberg bond orders (WBOs) of the Pd-C and Pd-P bonds as a function of  $J_{\text{Rh-P}}$  for the Pre-TS and TS of coupling between (B) EDOT/(C) benzene (oxidative addition substrate) and EDOT (arylation substrate). The solid lines represent WBOs at Pre-TS; the dotted lines represent those at TS. EE/PE indicates the CMD processes involving EDOT/benzene (oxidative addition substrate) and EDOT (arylation substrate). (D and E) The plot of the atomic orbital pair contribution of Pd(4d)-C(2p) to the Pd-C WBO and that of Pd(4d)-P(3p) to the Pd-P WBO as a function of  $J_{\text{Rh-P}}$  for the pre-TS and TS of the coupling between (D) EDOT/(E) benzene (oxidative addition substrate) and EDOT (arylation substrate). The solid lines represent the WBO contributions of the atomic orbital pair at Pre-TS; the dotted lines represent those at TS. Data for L6 were excluded from the linear  $J_{\text{Rh-P}}$  fit, as  $J_{\text{Rh-P}}$  failed to evaluate the L6 EDS due to the competitive interaction of its methoxy substituent. (F and G) The plots of the EDOT distortion energies as a function of the WBOs for the Pre-TS of the coupling between (F) EDOT/(G) benzene (oxidative addition substrate) and EDOT (arylation substrate). (H) The comparison between EDOT and Pre-TS EDOT in the second and fourth highest occupied molecular orbitals (HOMO-1 and HOMO-3). (I and J) The plots of the atomic orbital pair contribution of  $C_a(2pz)-C_b(2pz)$  to the  $C_\alpha-C_\beta$  WBO as a function of  $J_{\text{Rh-P}}$  for the pre-TS and TS of the reaction between (I) EDOT/(J) benzene (oxidative addition substrate) and EDOT (arylation substrate).



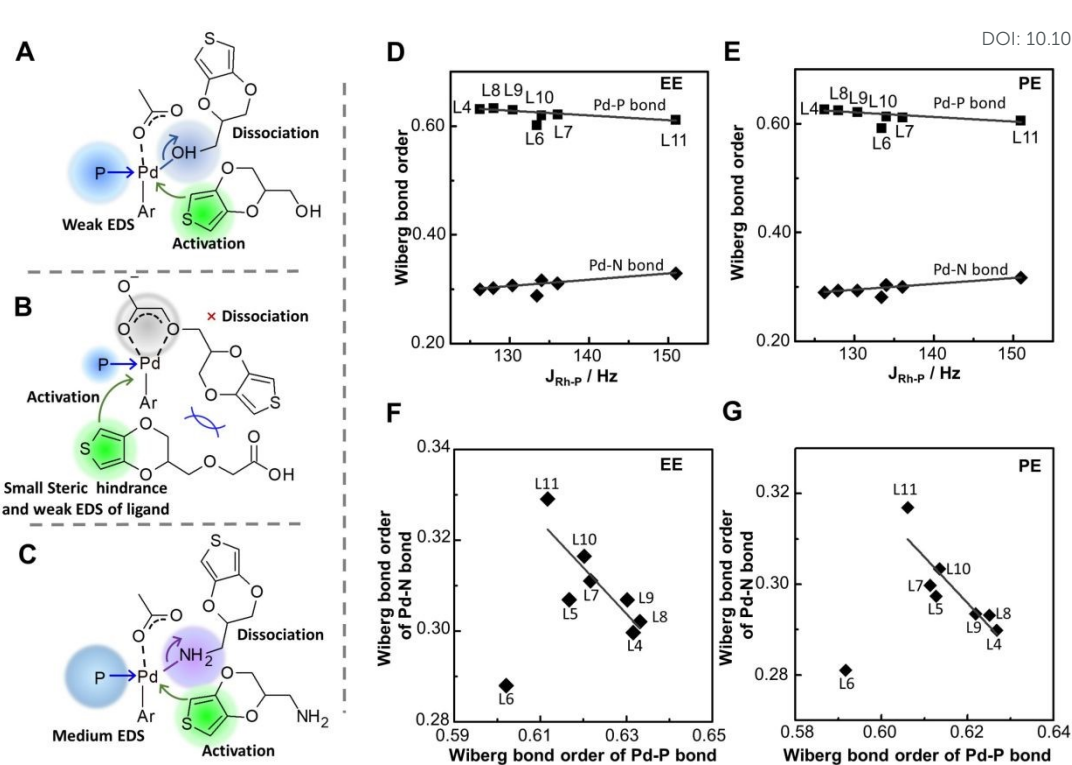


**Figure 5. Tuning ligand properties to achieve compatibility with polar side groups.** (A-C) The schematic presentations indicate (A) weak ligand coordination facilitates the C-H arylation of electron-rich EDOT-OH through strengthening the Pd-C bond and promoting deprotonation without the competitive coordination effect from hydroxyl groups due to their weak electron-donating strength (EDS), (B) a combination of weak ligand coordination and small ligand steric hindrance is necessary to activate EDOT-COOH due to the strong electrostatic association of COO<sup>-</sup> with palladium, and (C) a phosphine ligand with medium coordination can foster the dissociation of the mono-amine Pd(II) complex and subsequently deprotonation, thus effectively activating EDOT-NH<sub>2</sub>. (D and E) The plots for the Pd-N and Pd-P WBOs as a function of  $J_{Rh-P}$  for the mono-amine Pd(II) complexes involving (D) EDOT/(E) benzene (oxidative addition substrate) and EDOT-NH<sub>2</sub> (arylation substrate). The descriptions of EE and PE have been provided in Figure 4B and 4C. (F and G) The plot of the Pd-N WBO as a function of the Pd-P WBO for the mono-amine Pd(II) complexes involving (F) EDOT/(G) benzene (oxidative addition substrate) and EDOT-NH<sub>2</sub> (arylation substrate). The geometry of mono-amine Pd(II) complexes was optimized using M06L/6-31G(d) and SDD on Pd. The data of L6 was excluded from being used to fit the linear  $J_{Rh-P}$  dependence, as  $J_{Rh-P}$  failed to evaluate the L6 EDS due to the competitive interaction of its methoxy substituent.



## Data Availability Statement

The data supporting this study's findings are available from the corresponding author upon reasonable request.

Bo ZHU, PhD

Professor, Associate Dean

School of Materials Science and Engineering

Shanghai University

Email: [bozhu@shu.edu.cn](mailto:bozhu@shu.edu.cn) & [titbiam@gmail.com](mailto:titbiam@gmail.com)

